Emission-Line Properties of $z > 4$ Quasars [1,2]

Anca Constantin and Joseph C. Shields
Department of Physics and Astronomy, Ohio University, Athens, OH 45701

Fred Hamann
Department of Astronomy, University of Florida, Gainesville, FL 32611

Craig B. Foltz
MMT Observatory, Tucson, AZ 85721

Frederic H. Chaffee
W. M. Keck Observatory, Kamuela, HI 96743

ABSTRACT

High redshift QSOs provide important opportunities for advancing our understanding of the astrophysics of galaxy formation and evolution. Although a growing number of these sources are now known to exist at redshifts beyond 4, systematic studies of the emission-line properties of these objects are quite limited. We present results of a program of high signal-to-noise spectroscopy for 44 QSOs using the MMT and Keck observatories. The quasar spectra cover 1100 – 1700 Å in the rest frame for sources spanning a luminosity range of ~ 2 orders of magnitude. Comparisons between these data and spectra of lower redshift quasars reveal a high degree of similarity, although differences are present in the profiles and the strengths of some emission features. An examination of the luminosity dependence of the emission lines reveals evidence for a weak or absent Baldwin effect among $z \gtrsim 4$ QSOs. We compare measurements for objects in our sample with results from other high redshift surveys characterized by different selection techniques. Distributions of equivalent widths for these different ensembles are consistent with a common parent population, suggesting that our sample is not strongly biased, or in any case, subject to selection effects that are not significantly different from other surveys, including the Sloan Digital Sky Survey. Based on this comparison, we tentatively conclude that the trends identified here are representative of high z QSOs. In particular, the data bolster indications of supersolar metallicities in these luminous, high-z sources, which support scenarios that assume substantial star formation at epochs preceding or concurrent with the QSO phenomena.

Subject headings: quasars: emission lines—galaxies: abundances—galaxies:evolution

1. Introduction

The properties of QSOs at the highest known redshifts are important for understanding the

[1]Based in part on observations obtained at the MMT Observatory, a joint facility of the University of Arizona and the Smithsonian Institution.

[2]Based in part on observations obtained at the W.M. Keck Observatory, which is operated as a scientific partnership among the California Institute of Technology, the University of California and the National Aeronautics and Space Administration. The Observatory was made possible by the generous financial support of the W.M. Keck Foundation.

early history of galaxies and the formation of supermassive black holes. Over the past decade, a growing number of quasars have been reported at redshifts $z > 4$, corresponding in look-back time to more than $\sim 90\%$ of the age of the Universe. Objects in this regime are thus inherently young, and accordingly of great interest for studying the onset of accretion-powered activity in relation to galaxy formation and evolution.

Optical studies of QSOs at $z \gtrsim 4$ to date have mostly emphasized their discovery, luminosity function, and use as probes of intervening matter seen in absorption. Investigations of the emission-line properties of these objects have been far more limited (Schneider, Schmidt & Gunn 1991; Storrie-Lombardi et al. 1996). Further scrutiny of their emission spectra in relation to those of their low-redshift counterparts is clearly desirable. Specifically, such comparisons may reveal information on the timescale of star formation and chemical evolution associated with the QSO phenomenon (Hamann & Ferland 1999), and on time-dependent behavior of the accretion process (Mathur 2000).

This paper presents a detailed analysis of the optical emission line properties for a large sample of $z \gtrsim 4$ QSOs. High signal-to-noise, moderate resolution spectra of 44 quasars were obtained over multiple observing runs at the MMT and Keck observatories. The study employs direct measurements of the emisson lines as well as comparisons of composite spectra. Preliminary results from this survey were reported by Shields & Hamann (1997). Here we compare our spectra with those of redshift ~ 2 quasars and find general agreement, although subtle differences are present in the strengths and profiles of some emission features. Our objects show little evidence for a Baldwin Effect, the empirical anticorrelation between line equivalent width and luminosity L often found in lower redshift samples (Baldwin 1977; see Osmer & Shields 1999 for a review). We also investigate the degree to which our findings may be influenced by selection effects. We compare the properties of our targets with published measurements for other $z \gtrsim 4$ QSO samples representing a variety of discovery methods. This analysis indicates that our sources are representative of known quasars in this redshift regime, and suggests that the observed differences from lower-z sources are at least partially intrinsic. In subsequent papers (e.g., Dietrich et al. 2001), we will present more detailed comparisons of quasar emission-line properties as a function of redshift and luminosity, based on a sample of > 800 objects that span a much wider range in z and L.

Although the values of the adopted cosmological parameters play an important role at these extreme redshifts, we adopt throughout the paper an $H_0 = 50$ km s^{-1} Mpc^{-1}, $q_0 = 0.5$, $\Lambda = 0$ cosmology, to ease the comparison with earlier published work in this field.

2. Observations & data analysis

We began a program of spectroscopy of $z \gtrsim 4$ QSOs in 1994, with targets selected from the sources known at that time (~ 50) or reported in subsequent years in the literature. Data were obtained in a series of 7 observing runs at the MMT Observatory during 1994 – 1996, and 2 runs at the W. M. Keck Observatory in 1997 October and 1999 June. The goal of this program was to obtain a statistically significant description of quasar spectra in this high redshift regime; 32 objects were observed at the MMT, and 12 at Keck, for a total of 44 QSOs. Specific targets were selected based on their observability, with the brightest available sources given priority in order to maximize the resulting signal-to-noise ratio. We generally avoided sources known to exhibit strong absorption lines near the emission redshift. The majority of the observed objects are taken from the APM Color Survey (Storrie-Lombardi et al. 1996, BR/BRI prefix) and the Second Palomar Sky Survey (Kennefick et al. 1995b, PSS prefix). Table 1 lists the redshifts, r magnitudes, and the discovery reference for each source.

Data were acquired with the Red Channel of the MMT Spectrograph (Schmidt, Weymann & Foltz 1989) and with LRIS at the Keck II telescope (Oke et al. 1995). Observations were obtained with a long slit of 1″width, yielding full width at half maximum (FWHM) spectral resolution of ~ 10 Å and ~ 7 Å, with pixel sampling of 3.53 Å pixel^{-1} and 1.86 Å pixel^{-1}, respectively. These resolutions correspond to 300 – 400 km s^{-1} across the C IV λ1549 emission line, or typically 0.07 – 0.1 times this line's FWHM. The spectral coverage was chosen to span the redshifted Lyα λ1216 –

He II λ1640 interval; the He II feature is of specific interest since the N V λ1240/He II λ1640 ratio can be used as an abundance diagnostic (Hamann & Ferland 1993; Ferland et al. 1996). The observational setup was essentially identical for the two telescopes. A long-pass filter (LP495 at the MMT, GG495 at Keck) was used to prevent second-order contamination.

Multiple exposures totaling $\sim 1-2$ hrs were obtained for each quasar, yielding a typical signal-to-noise ratio of ~ 50 per pixel. Observations were obtained at an airmass $\lesssim 1.5$, and the slit was oriented approximately perpendicular to the horizon in order to minimize the effects of atmospheric differential refraction (Filippenko 1982). The atmospheric seeing was typically $1''$ (or better for the Keck II telescope), but not all the observations were obtained under absolute photometric conditions.

Calibration and reduction of the resulting spectra were carried out using standard techniques as implemented in the IRAF software package[3]. Observations of nearly featureless standard stars were used to provide flux calibrations and to correct for the atmospheric absorption bands. He-Ne-Ar arc-lamps were used for the wavelength calibrations. Multiple spectra acquired for the same object were averaged. Figure 1 presents all the reduced spectra included in this observational program, sorted on RA.

A small number of known Broad Absorption Line (BAL) QSOs were observed as part of the sample in order to enable additional comparisons with low-redshift quasars. These sources are PSS 1048+4407, BR 1144-0723, and PSS 1438+2538. Our spectra, which have greater S/N and wavelength coverage than many of the published discovery spectra, also reveal for the first time broad absorption lines in PC 0027+0525 and PSS 0137+2837.

The primary focus of the present work is on the emission lines. Accurate measurement of these features requires correction for absorption in many cases. For the majority of objects, the absorption appears as narrow lines due to associated or intervening systems, superimposed on either the emission lines or continuum. In these cases we removed the absorption feature through a simple interpolation. For the BAL QSOs and several additional objects (BRI 0151-0025, PSS 1159+1337, BRI 1346-0322, PC 1415+3408, and PSS 1435+3057), the absorption was severe enough that a reliable reconstruction of the unabsorbed spectrum was not possible. We excluded these sources from our measurements of the emission lines and from our composite spectra. All objects in this sample show strong Lyα forest absorption, which clearly influences the measured profile and flux of the Lyα emission line in many cases; we did not attempt to correct for this effect. Objects in our sample are subject to small amounts of Galactic foreground extinction, spanning $A_V = 0.04-0.49$, with a typical value of ~ 0.1 (Schlegel, Finkbeiner & Davis 1998). We corrected the spectra for the resulting reddening using the empirical selective extinction function of Cardelli, Clayton & Mathis (1989).

The spectra were Doppler-corrected to the rest frame using redshift values that we measured for the majority of sources from the C IV λ1549 line. The observed wavelength for each case was established by fitting a Gaussian to the top 20% of the profile. For situations where the measured line was significantly affected by absorption or low signal-to-noise, we verified the result with fits to the top 50% of the profile. For the BAL QSOs, the redshifts listed in Table 1 are taken from the discovery reference. For the remaining objects where C IV was not measurable due to absorption (see above), Lyα was used instead. The redshift measurements in these cases relied on Gaussian fits that used as a template only the red side of the profile. The resulting z determinations are in good agreement with previously published values, with an estimated uncertainty of ≤ 0.01.

Luminosities for our sample targets were derived using published photometric data. Rest-frame 1450Å fluxes (AB magnitudes at 1450Å) were obtained directly from the discovery papers for the majority of the objects in our sample. For the objects where these numbers were not available, the flux measured from our spectra was used, after the absolute flux calibration was adjusted to obtain consistency with published broad-band photometry. The luminosity values, expressed in ergs s^{-1} Hz^{-1}, are also included in Table 1.

[3]The Image Reduction and Analysis Facility (IRAF) is distributed by the National Optical Astronomy Observatories, which is operated by the Association of Universities for Research in Astronomy Inc. (AURA), under cooperative agreement with the National Science Foundation.

To investigate the emission-line properties of the observed QSOs, we constructed composite spectra, and employed measurements of the lines in individual objects.

The equivalent widths (EWs) of the strong lines, specifically for Lyα + N V and C IV λ1549, were measured interactively, using a direct integration of the line flux referenced to the interpolated continuum level. For the Lyα+N V feature we used the extension of the continuum from the red side only, and did not attempt any deblending. The resulting values for C IV are very similar to those obtained by modelling the lines with 2 Gaussians, representing broad and narrow components. Possible inaccuracies in these measurements are dominated by ambiguities in placement of the continuum; experiments with alternative choices of the continuum level suggest that this contributes a systematic uncertainty of $\sim 20\%$.

In our analysis, we found it useful to combine our measurements with published emission-line data for other $z \gtrsim 4$ QSO samples, and in particular those discovered via the Palomar CCD Grism Survey (Schneider, Schmidt & Gunn 1991, 1997; Schmidt, Schneider & Gunn 1995, hereafter referred to as SSG, ~ 15 objects), and early discoveries from the Sloan Digital Sky Survey (SDSS; Fan et al. 1999, 2000, 2001, ~ 35 objects, only those with $z > 3.9$ were considered in this analysis). In contrast with our measurements, the published EW values for these samples rely on single component Gaussian fitting. Our results and the published EWs can be meaningfully combined only if the line measurement procedures are consistent. We tested different methods of measuring the emission lines with our data. For the C IV line, the single Gaussian fits give, in general, lower EWs than those obtained with our direct integration technique, as they tend to lose flux from the wings if they are prominent, and from the peak if the cores dominate. In order to obtain a reasonable consistency in the comparisons involving the SSG and the SDSS samples, we measured the C IV EWs in both ways. For Lyα + N V, the fit results are sensitive to the method of treating the two lines and the asymmetry resulting from Lyα forest absorption; consequently, we employed only the EWs obtained by direct integration of the profile. The values are recorded in Table 1.

Finally, we constructed composite spectra using the data for individual sources normalized to unit mean flux over the wavelength range 1430 Å– 1470 Å. Average and median composites were calculated over the wavelength range common for all objects. The average composite may be influenced by several extreme objects with unusually strong and narrow lines (BR0401-1711, BRI1050-0000, BR2212-1626, BR2248-1242). The median spectrum may thus be more representative of the typical object in our sample.

3. Spectroscopic properties

3.1. General characteristics

An initial scrutiny of the spectra of $z > 4$ QSOs reveals substantial agreement with those of their lower redshift counterparts. This similarity is noteworthy, given the widely differing amounts of time available for the evolution of the AGN and underlying host galaxy. In Figure 2 (upper panel) we compare our $z \gtrsim 4$ average composite spectrum with the composite spectrum derived as an average[4] from the total *Large Bright Quasar Survey* (LBQS) sample, which is weighted toward $z \approx 2$ objects in this wavelength range (S. Morris 1999, private comunication; see Brotherton et al. 2001 for additional information). This comparison is especially useful given that our sample and the subset of the LBQS contributing to this wavelength interval have nearly identical average luminosities ($L_\nu(1450\text{Å}) \approx 31.3$), so that any differences should reflect a redshift dependence or differing selection criteria. We estimated the average LBQS $L_\nu(1450\text{Å})$ from the absolute B magnitude given by Francis et al. (1991), their Figure 8, following the methodology of Schneider, Schmidt & Gunn (1989) to relate the flux level in the two different bandpasses, while correcting for differences in cosmological parameters. In general terms, the high and intermediate redshift composites agree remarkably well; they have the same strong emission lines, similar continuum shape redward of the Lyα feature, and comparable strengths and profiles of the lines. The pronounced Lyα forest in the $z \gtrsim 4$ composites does not reflect an intrinsic difference in the nature of the emission sources, but rather an increase in the opacity of the inter-

[4]The algorithm used in constructing the LBQS composite is described by Francis et al. (1991)

galactic medium at larger redshifts.

Similarities between the QSOs at $z \gtrsim 4$ and those at lower redshift can also be seen in measurements of spectral features for individual sources. Surveys of QSOs at $z \approx 2-3$ (Francis et al. 1992; Francis, Hooper & Impey 1993) display strong (negative) correlations of line widths (FWHM) with line EWs and with line peak/continuum ratios. Similar tendencies are present in the high z sources. Figure 3 illustrates these results for all quasars in our sample, for which the C IV lines were measurable. Sources with narrow lines also tend to show the strongest emission. Furthermore, spectra of QSOs at $z \lesssim 3$ exhibit systematic line velocity shifts that correlate with the degree of ionization of the emitting species (Gaskell 1982; Espey et al. 1989; Tytler & Fan 1992; McIntosh et al. 1999). As reported previously by Storrie-Lombardi et al. (1996), this behavior is also present in $z > 4$ samples.

A detailed comparison of the high and intermediate redshift composites in Figure 2 shows excellent agreement for some lines but dissimilarities in others. C II λ1335 and Si IV+O IV] λ1400 remain basically unchanged, while differences are present in the strengths of Lyα, N V, C IV, and O I λ1304. The Lyα emission in $z \gtrsim 4$ quasars is considerably affected by the forest absorption, which may remove up to $\sim 50\%$ of the line, but the high-z composites nonetheless show a stronger Lyα feature than in the $z \approx 2$ average. The N V emission is also enhanced in the high z systems, and the same is true for the O I λ1304 emission. The rest-frame equivalent width of the latter feature is ~ 3Å in the composite $z \gtrsim 4$ spectra, which is about 50% larger than that seen in spectroscopic surveys at lower redshifts (e. g., Brotherton et al. 1994; Forster et al. 2000, EW(O I) ≈ 2Å).

The C IV line is stronger in the $z \gtrsim 4$ average than in the intermediate z composite spectrum. The difference is most pronounced in the line core, while the line wings are more nearly comparable in the two composites. As noted previously, the sample includes several remarkable objects with unusually strong and narrow lines, which potentially distort the comparison when using an average composite for this modest sample. To address this question, the high z median and the redshift ~ 2 composite are shown for comparison in Figure 2, lower panel. The Lyα and C IV features are clearly reduced in the high z median, but still stronger, especially in the core, than those in the LBQS composite.

Aside from the differences in Lyα and C IV, the high redshift median and average spectra are remarkably similar. In particular, the O I and N V emissions are equally strong in both high z composites. The degree of variation between the members of our sample can be seen in the standard deviation of the normalized spectra as a function of wavelength, plotted in Figure 4. The largest variations are present in the cores of the prominent emission lines (Lyα and C IV), consistent with the previous results for lower redshift samples (Francis et al. 1992; Brotherton et al. 2001). The lower panel of Figure 4 shows the standard deviation of the mean as a function of wavelength, which provides a measure of the uncertainty of the average spectrum.

3.2. O I and N V

The O I λ1304 and N V λ1240 lines show differences between the intermediate and high redshift spectrum composites that merit further attention. These features potentially convey information about the structure of the broad-line region and the physical conditions in the emitting plasma. Additionally, both lines are possible tracers of metallicity in the QSOs, which is of particular interest for understanding these sources in an evolutionary framework.

We first examine whether we have correctly identified the O I feature. Previous quasar emission line studies have raised the question of whether the λ1304 feature is indeed O I emission or something else. The O I line is a triplet (λ1302.17, λ1304.86, λ1306.03) with a mean laboratory wavelength (obtained by weighting each transition by its Einstein A coefficient) of 1303.50Å (Verner et al. 1996). For the high optical depths that may occur in broad line clouds, the individual features in the triplet will approach equal strengths, modifying the mean to 1304.36Å. The feature we attribute to O I is seen at a wavelength of $\sim$ 1307Å in these composites. At first glance, a better identification might seem to be with Si II $\lambda\lambda$1304.37, 1309.27 (mean laboratory wavelength 1307.63Å). However, this doublet is expected to be accompanied by considerable emission in other Si II lines, such as $\lambda\lambda$1196, 1264,

1531, 1817 (Gaskell 1982; Dumont & Mathez 1981), which are weak or absent. Furthermore, we note that the high z composites are derived from spectra that are Doppler-corrected using redshifts given by C IV, which is blueshifted relative to the low ionization lines. An identification of the λ1307 feature with O I would be consistent with this trend, while Si II would not. We conclude that the O I λ1304 identification is secure.

The enhanced strength of O I in the high redshift sources may reflect a structural difference in their broad-line regions (BLRs). Several studies of AGN ensembles suggest that low ionization lines (e.g. O I, C II) are emitted preferentially in low-velocity BLR components, while Lyα and high ionization lines (N V, Si IV, C IV) tend to trace higher velocity plasma (e. g., Brotherton et al. 1994; Francis et al. 1992; Wills et al. 1993; Baldwin et al. 1996). This is sometimes described in terms of a BLR with two components: the Intermediate Line Region (ILR) and Very Broad Line Region (VBLR). In our high redshift sample, the narrow component makes a larger fractional contribution to the spectra than in the lower redshift systems. The C IV line has a larger velocity width in the LBQS composite (FWHM $\approx$ 5600 km s^{-1}) than in the $z \gtrsim 4$ composites, both average and median (FWHM $\approx$ 4170 km s^{-1} and 4900 km s^{-1}, respectively). The unusual strength of O I emission may thus be the most obvious tracer of a characteristically enhanced ILR in $z > 4$ QSOs.

The strong N V emission is not expected in systems with an enhanced narrow component, however, because of its high ionization. The systematically higher N V emission may instead reflect high metallicity, consistent with standard chemical evolution scenarios for young, massive elliptical galaxies or galaxy bulges. Hamann & Ferland (1992, 1993) suggested that N V, which is a collisionally excited line, may be elevated relative to other lines as a consequence of the secondary nitrogen enrichment in vigorously star-forming environments. Interestingly, enhancements in the O I emission may provide supporting evidence for this interpretation. O I λ1304 is apparently formed via fluorescence with the H Lyβ line (see, e.g. Netzer 1990 for a discussion). The strength of the O I feature is thus expected to scale with the O/H abundance ratio (Netzer & Penston 1976). However, the O I line strength may be influenced by various other factors, such as the sensitivity of the line coincidence to the velocity field in the emitting region.

To summarize, the N V and O I features suggest that the broad-line regions of QSOs at $z > 4$ may be intrinsically different from those at lower redshift. Low-velocity components of the BLR are more prominent in these high-z sources, as signaled by the strength of O I and the narrow velocity width for C IV. In addition to this structural difference, however, the strength of N V emission implicates characteristically higher metallicities in the $z \gtrsim 4$ objects. High metallicities may also contribute to the enhancement of the O I line.

3.3. The EW vs. Luminosity correlation

To investigate the amplitude of the Baldwin Effect for QSOs at $z \gtrsim 4$, we present plots of the rest equivalent width of C IV λ1549 as a function of the continuum luminosity L_ν (measured at 1450 Å in the rest frame), for our observed sample (Figure 5, upper panel), and for an enlarged sample that includes also measurements obtained from the SSG and SDSS surveys (Figure 5, lower panel). The dotted line is the relation found by Osmer et al. (1994) for a sample of 186 quasars covering a wide range of redshift ($z < 3.8$). The overall results at high redshift ($z > 4$) appear compatible with the trend and scatter found for AGNs at lower redshift and luminosity, but do not, by themselves, show a Baldwin Effect correlation in C IV. A Spearman test is consistent with the null hypothesis at $> 99\%$ level. The corresponding diagrams for Lyα + N V are shown in Figure 6, and likewise are consistent with no correlation. These measurements combine Lyα and N V, and therefore, a possible trend in the Lyα line alone, for which the Baldwin Effect has been previously claimed, may be weakened by the presence of N V, which does not show such $EW - L_\nu$ anticorrelation (Osmer, Porter & Green 1994; Korista et al. 1998).

To explore further the luminosity-dependent behavior, we divided the quasars in our sample into two luminosity bins, with log L_ν(1450 Å) $= 30.34 - 31.12$ and $31.31 - 31.97$. Average and median composites for these subsets are shown in Figure 7. The noise and the intrinsic peculiarities present in single sources are considerably diminished in the composite spectra, making them a valuable tool in identifying line strength variations

originating in differences in luminosity. A simple inspection of the individual lines reveals a small decrease in the EW with luminosity for Lyα, but not for C IV or other emission lines.

The weak or absent Baldwin Effect in our $z \gtrsim 4$ sample may be an intrinsic characteristic of these objects, which are extreme in both redshift and luminosity. Alternatively, the absence of a clear trend may stem from the limited luminosity range of our sample and the substantial scatter that always appears in the $L_\nu - EW$ relation. Selection effects influencing our sample are also a significant concern; if strong-lined objects are over-represented among our high luminosity QSOs, the result would be a weakened Baldwin correlation. We explore the role of selection effects further in the next section.

3.4. Selection biases

An important consideration in interpreting the properties of our high redshift QSOs is the extent to which selection effects can influence the properties of a sample. Here we examine the methods used for identifying $z \gtrsim 4$ QSOs and ways that selection criteria may be reflected in emission-line characteristics.

The majority of QSOs known at $z > 4$ have been discovered by color-selection techniques (Irwin et al. 1991; Kennefick et al. 1995a,b; Storrie-Lombardi et al. 1996, 2001) that rely in particular on the contrast between the observed spectral region centered on the Lyα feature, and the continuum at shorter wavelengths, which is strongly absorbed by the Lyα forest. Quasars are thus distinguished from stars primarily on the basis of their extremely red B – R or similar colors, which separate them from the stellar locus in the color-magnitude/color-color diagrams. The emission lines can contribute significantly to the total flux observed in typical photometric bandpasses. Their role is amplified at these particularly high redshifts since the scaling factor $(1+z)$ boosts the values of the observed EWs.

The prominence of Lyα could therefore introduce biases affecting the detectability of $z \gtrsim 4$ quasars. Most of the objects in our sample come from the APM Color Survey (BR/BRI quasars). These quasars are drawn from a magnitude-limited sample, and as a consequence, the strong-lined sources could be over-represented because of the contribution of the Lyα line to the measured flux in the R band (Malmquist bias). The amplitude of this effect can be roughly evaluated by estimating the change in the apparent (R) magnitude produced by the presence of a strong Lyα line: for a rest frame $\mathrm{EW}_1 = 30$Å (weak line) and $\mathrm{EW}_2 = 160$Å (strong line) with respect to the unabsorbed continuum, the observed ($z \approx 4.5$) equivalent widths would be $\mathrm{EW}_1^{obs} \approx 165$ Å and $\mathrm{EW}_2^{obs} \approx 880$ Å respectively. With an R bandpass of width ~ 1000 Å, the line increases the measured flux by $\sim 16\%$ and 88% compared with a pure continuum source. The ratio of the two broadband fluxes with strong compared to weak Lyα would be $f_2/f_1 \simeq 1.62$, which corresponds to a difference in magnitude $\simeq 0.5$ mag. This value is actually an underestimate of the effect because the continuum blueward of Lyα is highly suppressed by the absorption forest. In addition, for some of the observations in the BRI survey, a narrower R bandpass (~ 600Å) was used, resulting in an increase of the fractional contribution of Lyα to the measured flux. This effect leads to a bias in favor of objects with large EW, that could potentially account for the unusual examples of strong-lined QSOs in our sample. The same trend was suggested previously by Kennefick et al. (1995b), who calculated the selection probabilities of QSOs (from POSS II observations) for three cases of Lyα + N V line strength (see their Fig. 6). These considerations apply to the BR/BRI, PSS, and SDSS sources, which rely on similar bandpasses for QSO identification.

Although this effect seems to be important, it could be counteracted by the treatment of the other bandpasses in the selection process. If only sources that are detected in B are included, as is the case for the APM survey, objects with very strong lines near the limiting R magnitude may be excluded, because their R-band flux is dominated by Lyα and the continuum (which dominates in B) is correspondingly weak. However, the selection process is further affected by the fact that, for very weak lines, the contrast between the Lyα emission and the continuum blueward of it may not be high enough to satisfy the necessary color criterion. In the case of the APM survey, the understanding of this bias is complicated by the use of a magnitude-dependent color threshold, due to signal-to-noise

considerations (Storrie-Lombardi et al. 2001, see their Figure 1), again introducing a preference for strong-lined sources. The fact that the majority of the color selected objects in our sample fall above the dotted line in the Baldwin diagram, may be due, in part, to this bias.

A thorough understanding of the Malmquist and color biases would require extensive modeling based on the choices of filters, limiting magnitudes, and/or colors. An alternative is to investigate the EW properties of samples discovered by different techniques. We compared the EWs and composite profiles of our color-selected sources to a grism-selected sample, which includes objects observed by us and by Schneider, Schmidt & Gunn (1991). The SSG sample consists of quasars selected based on the detection of Lyα in slitless spectra. As discussed by Schmidt, Schneider & Gunn (1995), this detection technique may also lead to preferential selection of QSOs with strong lines. Figure 8 shows the rest-frame and the observed EW distributions, for C IV and Lα, for the color-selected and grism-selected samples. The K-S (Kolmogorov-Smirnov) statistics are consistent with the two samples having the same parent population. The average and median composite spectra should indicate similar trends. Figure 9 shows this comparison, which reveals a remarkable similarity between the composites. Likewise, there is no apparent difference in N V and O I; both lines are evidently stronger in the high redshift sources, regardless of the selection technique. We can conclude that the color selection methods (primarily BR/BRI) find QSOs with analogous properties to those of sources found by the SSG grism survey. Therefore, the corresponding biases, if apparent, affect the samples to a similar degree.

More useful comparisons may be those with the SDSS sample, which is claimed to be less biased. According to the authors, the selection probability in the SDSS detection of high redshift objects does not strongly depend on the emission line strength, but on the redshift and the SED shape. Comparisons between observed EW(Lyα) distributions for our sample, the grism (SSG) sample and the SDSS survey show that they are consistent with a single distribution function (probability of being drawn from the same distribution is respectively $\mathrm{KS}_{SDSS/oursample} = 0.633$, $\mathrm{KS}_{SDSS/grism} = 0.910$). The rest and observed frame EW histograms, for both Lyα and C IV, are displayed in Figure 8, separately for color-selected QSOs from our sample, for the grism-selected objects from SSG, and for the SDSS quasars. The KS statistic in each case is consistent with a common parent population.

One possible complication in this comparison may be that the characteristic luminosities for these different samples are not the same. Inspection of Figures 5 and 6 indicate that quasars in our sample are somewhat more luminous than those in the SDSS. The Baldwin Effect would then predict smaller EWs for our sources. The fact that the EW distributions are actually similar could thus be a coincidence, due to a bias favoring strong-lined objects in our sample. A closer inspection of the luminosity distributions suggests that such a conspiracy is unlikely to be significant. There is substantial overlap in luminosities for the different samples, and differences in their median values are small; median L_ν for our QSOs exceeds that of the SDSS sources by only a factor of 2.

We conclude that the selection effects, if present, are not more evident in our sample than in the other high redshift surveys.

4. Discussion

Interpretations of the strong cosmological evolution of AGNs are generally based on the functional form of a (simple) observed luminosity function of bright QSOs at high z and prescriptions for the growth and luminosity of the underlying black holes. In the cold dark matter scenario, as a paradigm for a hierarchical cosmogony that models the evolution of the luminosity function, quasars are believed to be a short-lived, first phase of the formation of a galaxy in the potential well of a dark matter halo (Haehnelt & Rees 1993; Haiman & Loeb 2001).

Observations at high redshifts intercept epochs when quasars are very young objects, which thus might be expected to have characteristically low metallicity. However, the trends reported here in the N V and O I broad emission lines (section 3.2) suggest that the metallicities are typically higher in higher redshift, and implicitly more luminous QSOs. The prominent emission lines indicate that, in spite of their youth, the high-redshift QSOs have undergone substantial chemical enrich-

ment on a timescale that is short compared with their life span, implying a rapid star formation process in the host galaxy. Therefore, the very existence of objects at $z > 4$ presents severe timing problems (time to form and turn on), that can be solved only under the assumption that they reside in the most massive objects which have collapsed at these early epochs, associated with the rare high peaks in the primordial density field (Turner 1991; Katz et al. 1994). This result may naturally arise from the analogy with the mass-metallicity relationship present in the low z spirals and ellipticals: massive galaxies reach higher metallicities because their deeper potential is better able to retain their gas against the galactic winds built by the thermal pressure from supernovae, while low-mass systems eject their gas before high enrichments are attained. Thus, quasar metallicities should be similarly tied to the gravitational binding energy of the local star-forming regions, and perhaps also to the total mass of their host galaxies (Hamann & Ferland 1999).

Consistent with this picture, recent AGN studies have revealed correlations between the mass of the central black hole and QSO luminosities, QSO host masses, and the stellar velocity dispersion (Laor 1998; Magorrian et al. 1998; Ferrarese & Merritt 2000; Gebhardt et al. 2000). Quasar broad lines trace matter within only the central few parsecs, but the emerging black hole/bulge connections strongly suggest that the emission-line plasma is closely linked to the larger star-forming environment. Recent cosmic-structure simulations (Gnedin & Ostriker 1997) show that protogalactic condensations can form stars and reach higher than solar metallicities at $z \gtrsim 6$, suggesting that at epochs preceding, or concurrent with the QSO formation period, the bulge star formation already occurred. Therefore, interpretation of the abundance data in these extreme redshift sources yields unique constraints on the evolution of those environments, indirectly probing the epoch and extent of early star formation associated with QSOs. The observed enhancements in the N V and O I emission reinforce the previous evidence of solar or greater metallicities ($Z > Z_{\odot}$) that occur before QSOs become observable (Dietrich & Wilhelm-Erkens 2000; Hamann & Ferland 1999 and references therein).

The evidence of structural differences reported in Section 3.2 for the broad line region in these young sources provides further motivation for examining their evolutionary context. If the enhanced ILR emission is real and not a consequence of selection effects, this behavior may be an important tracer of accretion physics and its relationship to redshift and luminosity. Based on our initial reports of narrow UV lines in $z \gtrsim 4$ QSOs, Mathur (2000) suggested an analogy between these sources and narrow-line Seyfert 1 (NLS1) galaxies. In this picture, both classes of objects are in an early evolutionary phase, in which accretion proceeds at or near the Eddington limit. While this scenario has several appealing aspects for explaining NLS1 phenomena, assigning it in general to high-z QSOs may be premature. While the latter sources are young in cosmological terms (ages $\lesssim 2$ Gyr), this does not ensure that they are in an early phase of accretion, since the timescale for QSO activity in an individual source is estimated to be only a few times 10^7 yr (e.g., Kauffmann & Haehnelt 2000). Furthermore, narrow profiles in the UV lines are probably not an adequate basis for linking our sources to a NLS1 classification, which is based on optical lines. As discussed by Wills et al. (2000), the UV line widths do not correlate in a simple way with Hβ width or with other NLS1 properties. Further inquiry is needed to understand the implications of line profile behavior in high-redshift QSOs.

5. Conclusions

Although an increasing amount of information is becoming available on the properties of QSOs discovered at very high redshift, only limited efforts have been made to survey systematically the emission-line properties of these objects and/or the selection effects related with the techniques by which they were discovered. We have conducted a thorough analysis of 44 high signal-to-noise spectra from the MMT and Keck observatories which yield measurements of the most prominent emission lines in the rest-frame interval 1100Å – 1700Å.

Composite spectra for the whole data set and for subsets were constructed and analysed in order to investigate: a) the emission properties of $z \gtrsim 4$ QSOs in comparison with those of their lower redshift counterparts, b) the luminosity dependence of the emission features, and c) the role of selec-

tion effects in existing samples. There are several conclusions that may be inferred from the work we have outlined here:

1. In terms of their ultraviolet rest-frame spectra, $z \gtrsim 4$ QSOs strongly resemble quasars at low redshift. Subtle differences are present, however, and in particular, Lyα, N V, C IV and O I are stronger in the high z sources. The C IV line is also systematically narrower in the $z \gtrsim 4$ objects.

2. Among the high redshift QSOs, a weak Baldwin Effect is possibly present in Lyα but not in C IV or other lines. The lack of a strong trend may reflect the limited span of luminosity in the existing $z \gtrsim 4$ samples.

3. Selection effects favoring strong-lined objects are a significant concern for surveys of high redshift QSOs. Our sample includes several sources with extremely strong, narrow and peaked lines that may arise from such a bias. However, quantitative comparisons with other existing surveys of $z \gtrsim 4$ QSOs, including those discovered by SDSS, suggest that our sample overall is not strongly biased in this way.

4. All $z > 4$ composite spectra show strong N V and O I. The unusual strengths of these features and the narrow C IV profile suggest the presence of characteristic structural differences in the BLR, and also high abundances of heavy elements (solar or up to several times solar metallicities) in quasar environments at these early times. These findings are consistent with standard chemical evolution scenarios for young, massive bulge-dominated galaxies.

We thank Matthias Dietrich, George Djorgovski, Julia Kennefick, and Lisa Storrie-Lombardi for helpful conversations and for making their results available in advance of publication. We are grateful to Don Schneider for providing us with the SSG spectra in digital form, and for answering questions concerning grism selection methods. We thank our referee, Paul Francis, for valuable comments that resulted in improvements in the manuscript. Financial support for this research was provided by the National Science Foundation through grants AST 98-03072 to C.B.F. and AST 99-84040 to F.H. The authors wish to extend special thanks to those of Hawaiian ancestry on whose sacred mountain we are privileged to be guests. Without their generous hospitality, many of the observations presented herein would not have been possible.

REFERENCES

Baldwin, J.A. 1977, ApJ, 214, 769

Baldwin, J.A., et al. 1996, ApJ, 461, 664

Becker, R. H., Helfand, David J., & White, R. L. 1992, AJ, 104, 531

Brotherton, M. S., Wills, B. J., Francis, P. J., & Steidel, C. C. 1994, ApJ, 430, 495

Brotherton, M. S., Tran, Hien D., Becker, R. H., Gregg, Michael D., Laurent-Muehleisen, S. A., & White, R. L. 2001, ApJ, 546, 775

Cardelli, J. A., Clayton, G. C., & Mathis, J. S. 1989, ApJ, 345, 245

Dickinson, M., & McCarthy, P. J. 1987, BAAS, 19, 1125

Dietrich, M., & Wilhelm-Erkens, U. 2000, A&A, 354, 17

Dietrich, M., et al. 2001, in preparation

Dumont, A. M., & Mathez, G. 1981, A, &A 102, 1

Espey, B. R., Carswell, R. F., Bailey, J. A., Smith, M. G., & Ward, M. J. 1989, ApJ, 342, 666

Fan, X., et. al 1999, AJ, 118, 1

Fan, X., et al. 2000, AJ, 119, 1

Fan, X., et al. 2001, AJ, 121, 54

Ferland, G. J., et al. 1996, ApJ, 461, 664

Ferrarese, L., & Merritt, D. 2000, ApJ, 539, L9

Filippenko, A. V. 1982, PASP, 94, 715

Forster, K., Paul J. G., Aldcroft T. L., Vestergaard M., Foltz G. B., & Hewett P. C. 2001, ApJS, in press

Francis, P. J., Hewett, P. C., Foltz, C. B., Chaffee, F. H., Weymann, R. J., & Morris, S. L. 1991, ApJ, 373, 465

Francis, P. J., Hewett, P. C., Foltz, C. B., & Chaffee, F. H. 1992, ApJ, 398, 476F

Francis, P. J., Hooper, E. J., & Impey, C. D. 1993, AJ, 106, 417

Gaskell, C. M. 1982, ApJ, 263, 79

Gebhardt, K., et al. 2000, ApJ, 539, L13

Gnedin, N. Y., & Ostriker, J. P. 1997, ApJ, 486, 581

Haehnelt, M. G., & Rees, M, J. 1993, MNRAS, 263, 168

Haiman, Z., & Loeb, A. 2001, in press

Hamann, F., & Ferland, G. 1992, ApJ, 391, L53

Hamann, F., & Ferland, G. 1993, ApJ, 418, 11

Hamann, F., & Ferland, G. 1999 ARA&A, 37, 487

Henry, J. P., et al. 1994, AJ, 107, 127

Irwin, M., McMahon, R. G., & Hazard, C. 1991, in ASP Conf. Ser. 21, The Space Distribution of Quasars, ed. D. Crampton (San Francisco: ASP), 117

Isaak K. G., McMahon, R. G., Hills, R. E., & Withington, S. 1994, MNRAS, 269, 28

Katz, N., Quinn, T., Bertschinger, E., & Gelb, J. M. 1994, MNRAS, 270, L71

Kauffmann, G., & Haehnelt, M. 2000, MNRAS, 311, 576

Kennefick, J. D., et al. 1995a, AJ, 110, 78

Kennefick, J. D., Djorgovski, S. G., & de Carvalho, R. R., 1995b, AJ, 110, 2553

Kennefick, J. D., Djorgovski, S. G., & Meylan, G., 1996, AJ, 111, 1816

Korista, K., Baldwin, J., & Ferland, G. 1998, ApJ, 507, 24

Laor, A. 1998, ApJ, 505L, 83L

Magorrian, J., et al. 1998, AJ, 115, 2285

Mathur S. 2000, MNRAS, 314, 17

McIntosh, D. H., Rix, H.-W., Rieke, M. J., & Foltz, C. B. 1999, ApJ, 517, 73

Netzer, H. 1990, in Active Galactic Nuclei, ed. T. J.-L. Courvoisier, & M. Mayor (Berlin: Springer), 57

Netzer, H., & Penston, M. V. 1976, MNRAS, 174, 319

Oke, J. B., et al. 1995, PASP, 107, 375

Osmer, P. S., Porter, A. C., & Green, R.F. 1994, ApJ, 436, 678

Osmer, P. S., & Shields, J. C. 1999, ASP Conf. Ser.162, Quasars and Cosmology, ed. G. Ferland, & J. Baldwin (San Francisco: ASP), 235

Shields, J. C., & Hamann, F. 1997, RevMexAA (Serie de Conf.), 6, 221

Schlegel, D. J., Finkbeiner, D. P., & Davis, M. 1998, ApJ, 500, 525

Schmidt, G. D., Weymann, R. J., & Foltz, C. B. 1989, PASP, 101, 713

Schmidt, M., Schneider, D. P., & Gunn, J. E. 1987, ApJ, 316, L1

Schmidt, M., Schneider, D. P., & Gunn, J. E. 1995, AJ, 110, 68S

Schneider, D. P., Schmidt, M., & Gunn, J. E. 1989, AJ, 98, 1507

Schneider, D. P., Schmidt, M., & Gunn, J. E. 1991, AJ, 101, 2004

Schneider, D. P., Schmidt, M., & Gunn, J. E. 1997, AJ, 114, 36

Smith, J. D., Thompson, D., & Djorgovski, S. G. 1994a, AJ, 107, 24

Smith, J. D., et al. 1994b, AJ, 108, 1147

Storri-Lombardi, L. J., McMahon, R. G., Irwin, M. J., & Hazard, C. 1996, ApJ, 468, 121S

Storri-Lombardi, L. J., Irwin, M. J., McMahon, R. G., & Hook, I. M. 2001, MNRAS, 322, 933S

Turner, E. L. 1991, AJ, 101, 1

Tytler, D., & Fan, X. M. 1992, ApJS, 79, 1

Verner, D. A., Verner, E. M., & Ferland, G. J. 1996, Atomic Data Nucl. Data Tables, 64, 1

Wills, B. J., Brotherton, M. S., Fang, D., Steidel, C. C., & Sargent, W. L. W. 1993, ApJ, 415, 563

Wills, B. J., Shang, Z., & Yuan J. M. 2000, New Astronomy Reviews, 44, 511

AAS LaTeX macros v5.0.

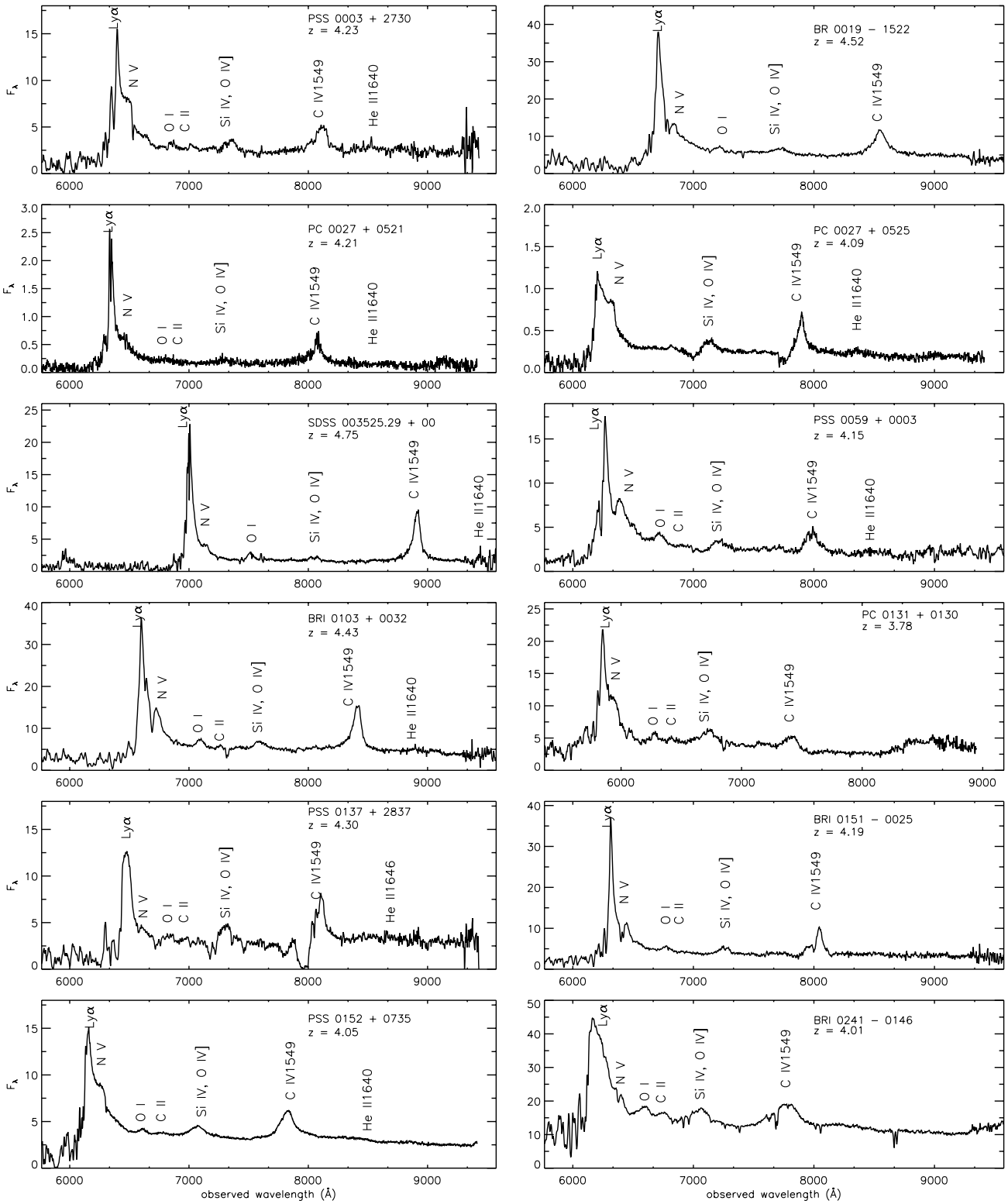

Fig. 1.— Observed spectra of QSOs at $z \gtrsim 4$. The flux, F_λ, is in units of 10^{-17} erg s^{-1} cm^{-2} Å^{-1}. The prominent emission features are marked.

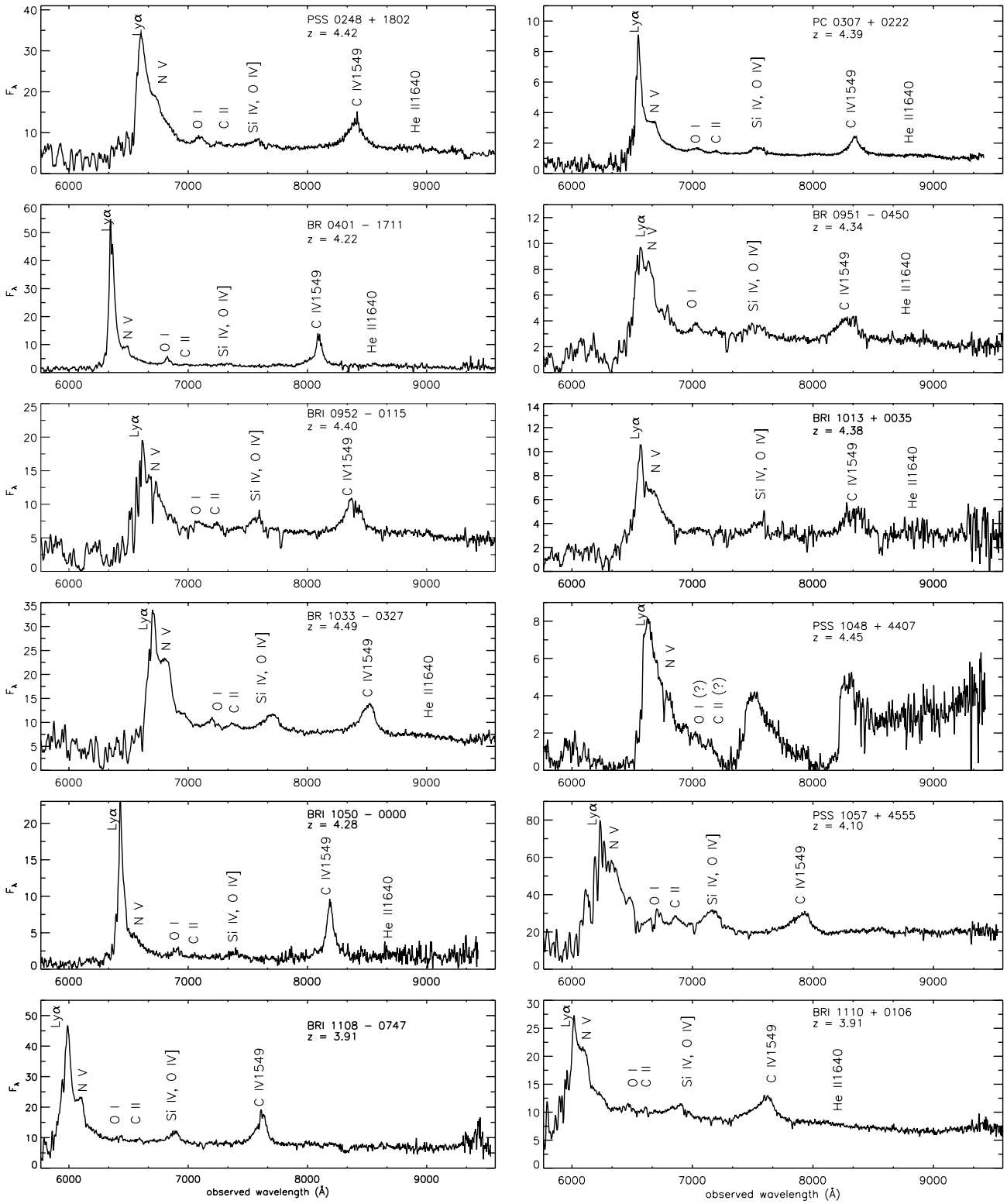

Fig. 1 continued.—

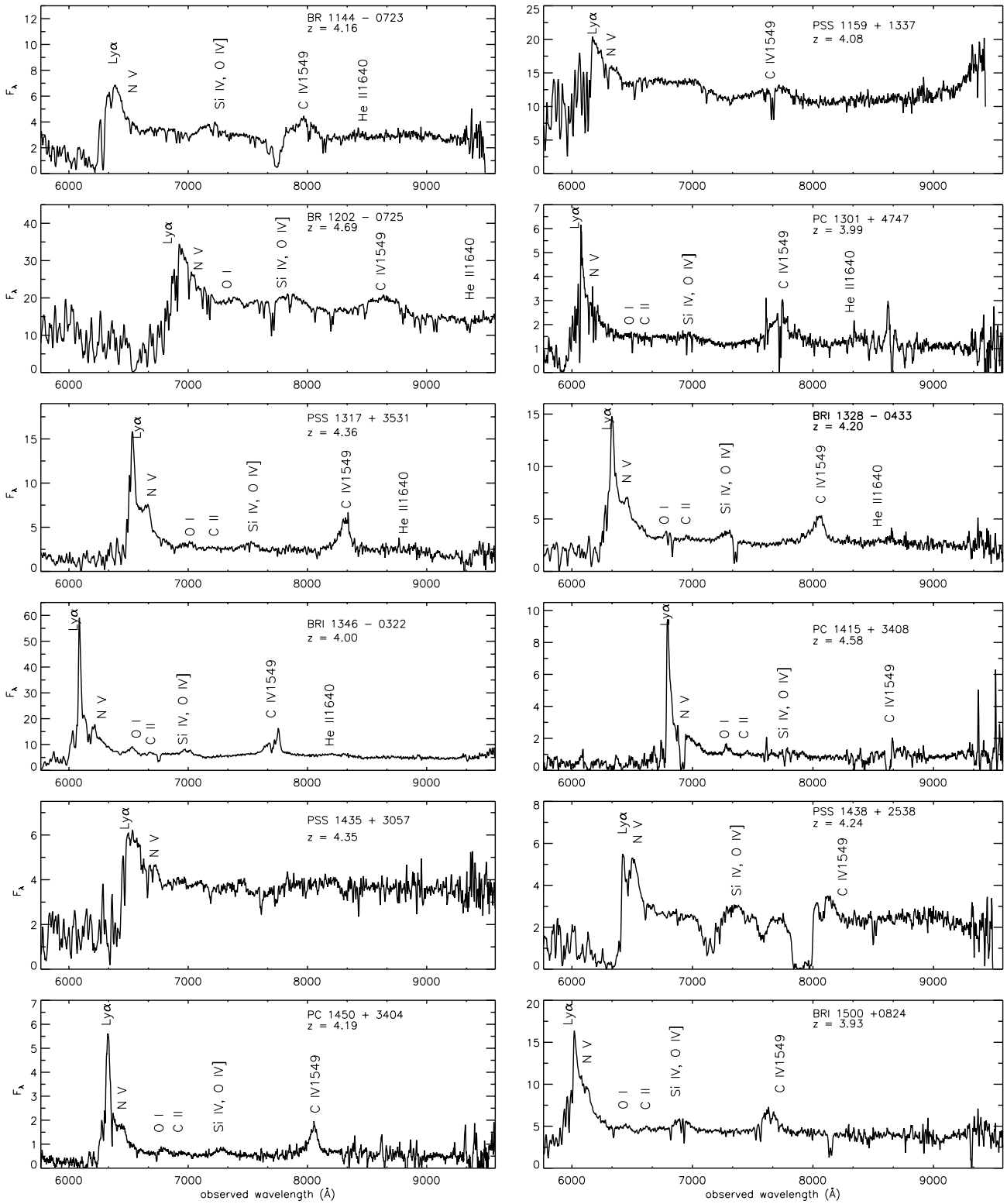

Fig. 1 continued.—

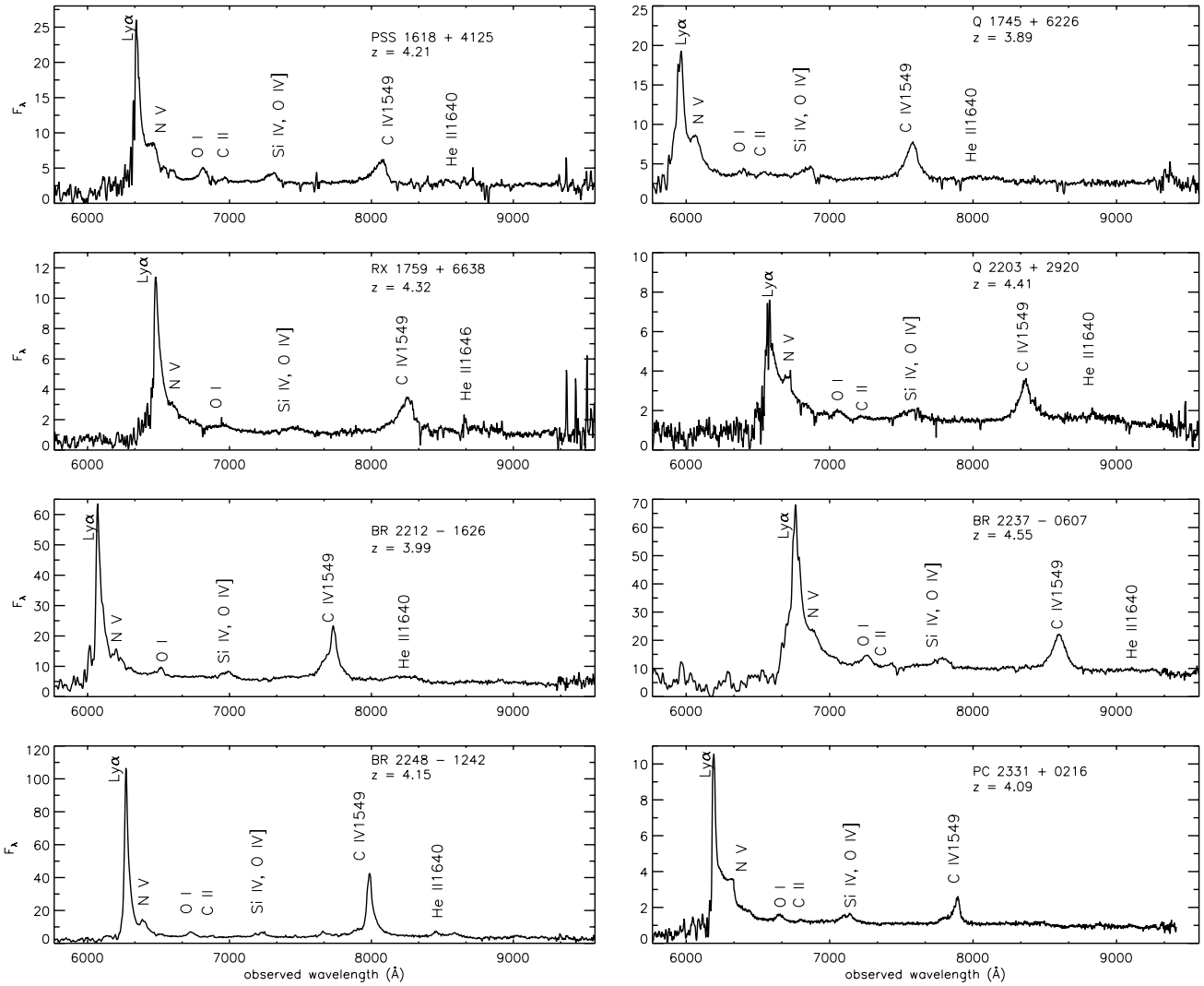

Fig. 1 continued.—

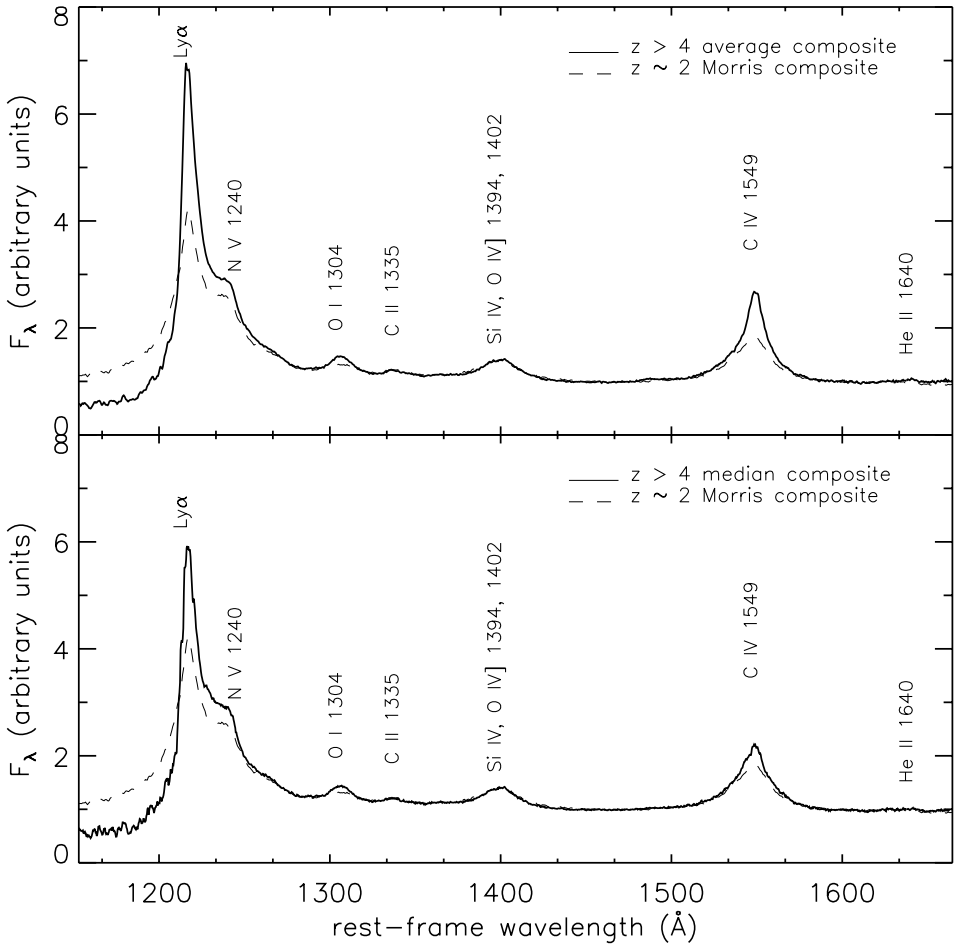

Fig. 2.— Composite spectra (average -upper panel, and median -lower panel) of $z \gtrsim 4$ QSOs included in this observational program are shown in comparison with the LBQS composite, representative of $z \approx 2$ objects. The y-axis has been normalized to unit mean flux over the wavelength range 1430 Å– 1470 Å. The redshift measured from the C IV feature was used for the Doppler correction of the $z \gtrsim 4$ spectra. As a consequence of the different velocity shifts presented by the low- and high-ionization lines, the alignment of the high-z spectral features with those in the low z composite required a slight additional shift of our composites.

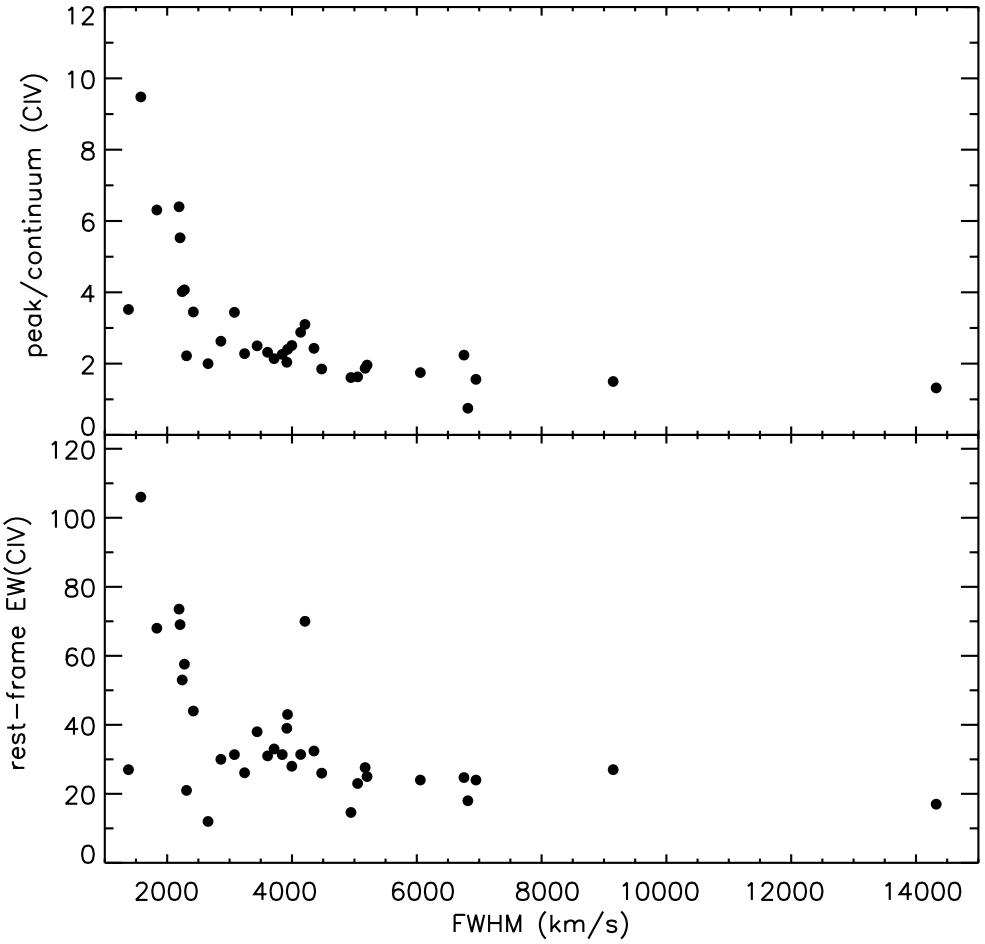

Fig. 3.— Equivalent widths and line peak/continuum ratios for C IV emission as a function of C IV line widths (full width at half maximum, FWHM), measured in our sample.

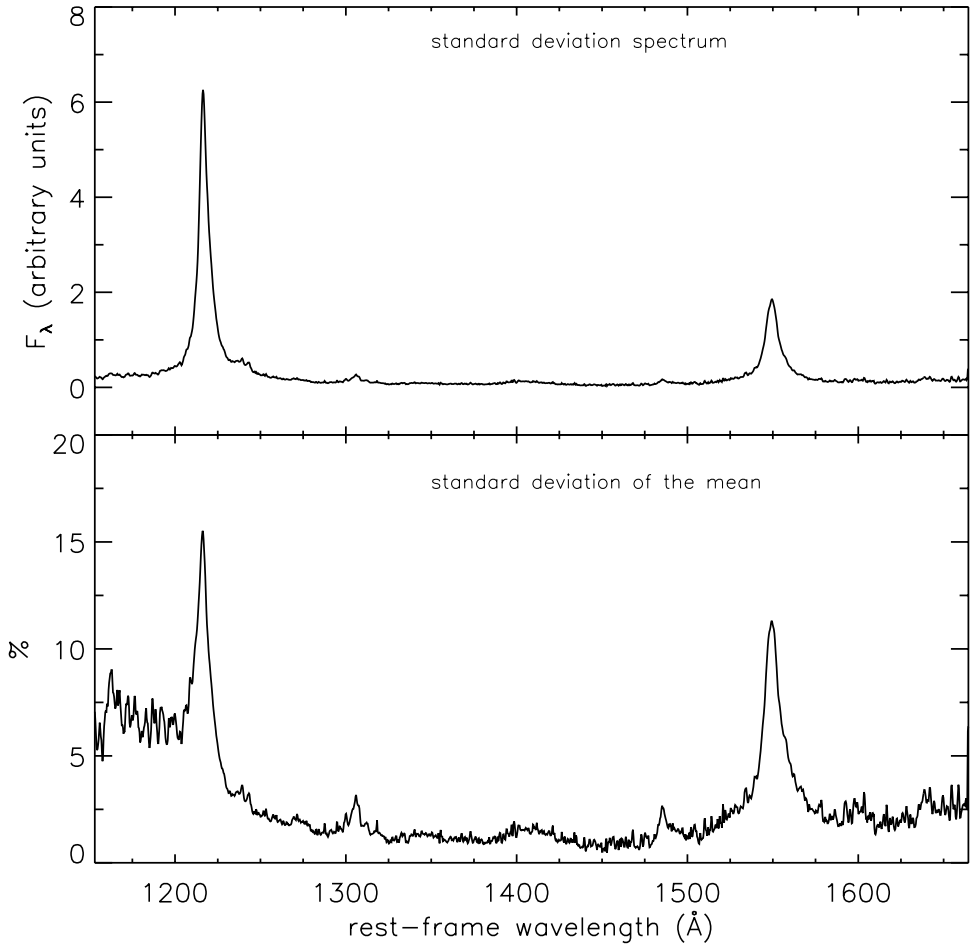

Fig. 4.— Upper panel: Flux standard deviation in F_λ relative to the average composite spectrum, as a function of wavelength for the individual spectra comprising the composites. Lower panel: The standard deviation of the mean, expressed in %.

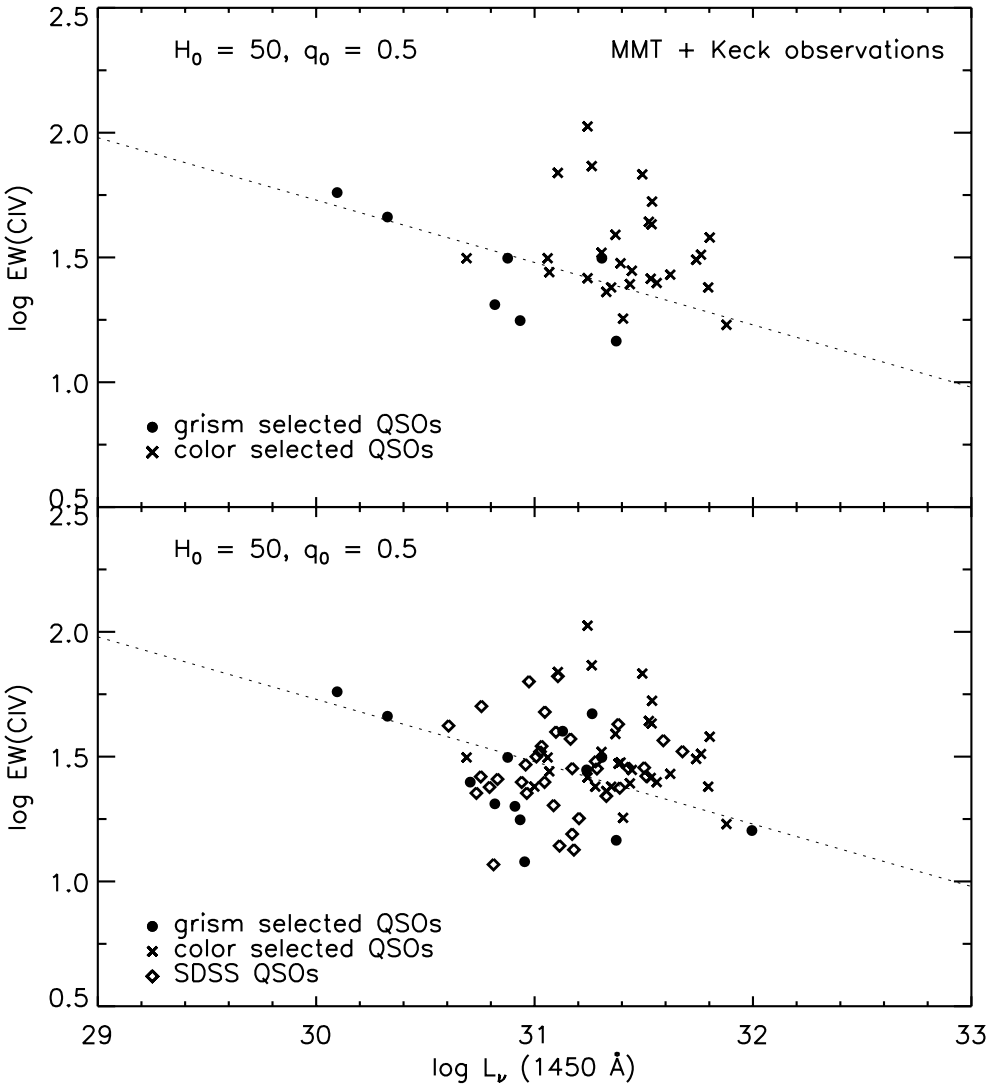

Fig. 5.— Rest-frame EW of the C IV emission line as a function of absolute luminosity of the quasar (at 1450 Å rest frame). The Baldwin Effect reported by Osmer, Porter & Green (1994), based on measurements at lower redshift, is shown by the dotted line. The upper panel shows measurements from our sample only, with different symbols for the color (×) and grism (•) selected objects. The lower panel adds measurements for $z \gtrsim 4$ QSOs from Schneider, Schmidt & Gunn (1991) and the SDSS survey. Although consistent with the low redshift trend, the measurements do not, by themselves, show the expected correlation.

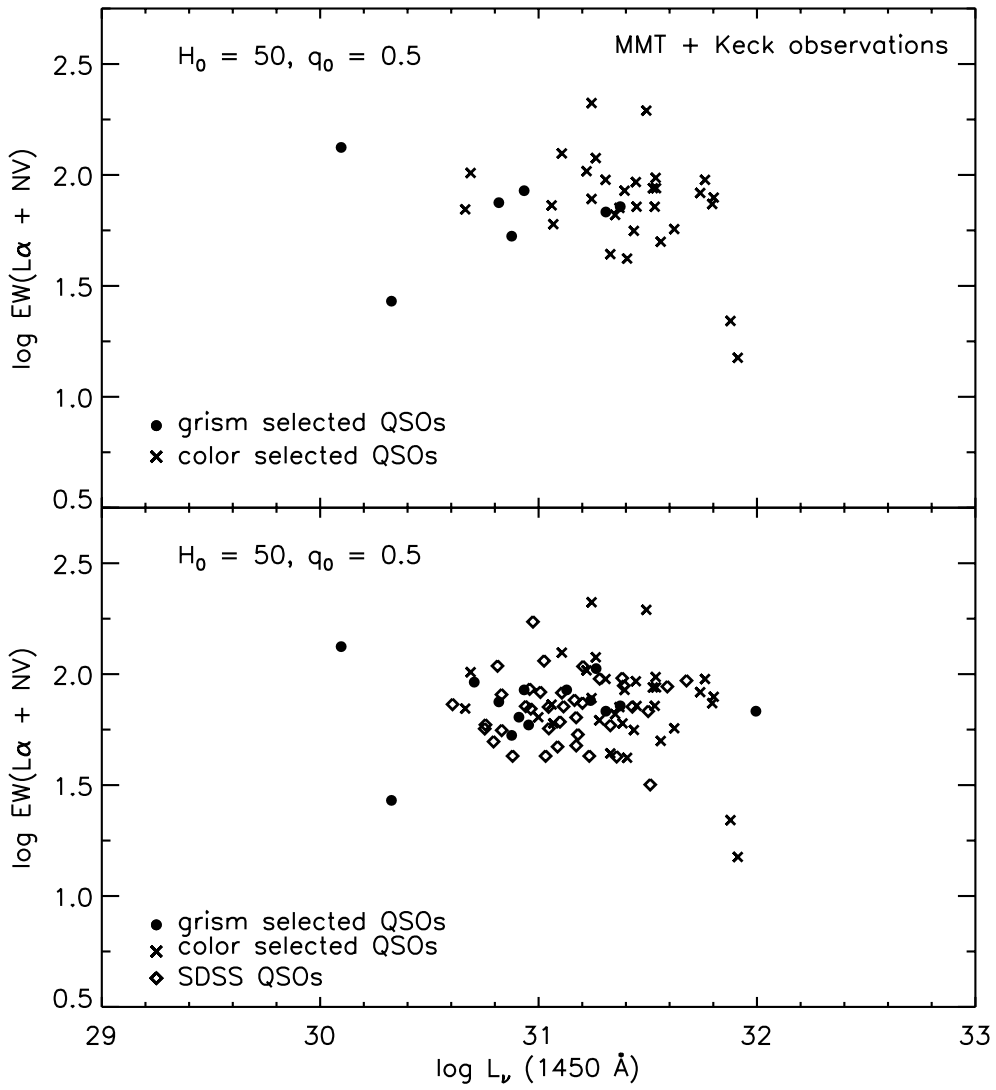

Fig. 6.— Equivalent width of Lyα + N V versus continuum luminosity for $z \gtrsim 4$ QSOs. Symbols are the same as in Fig. 5.

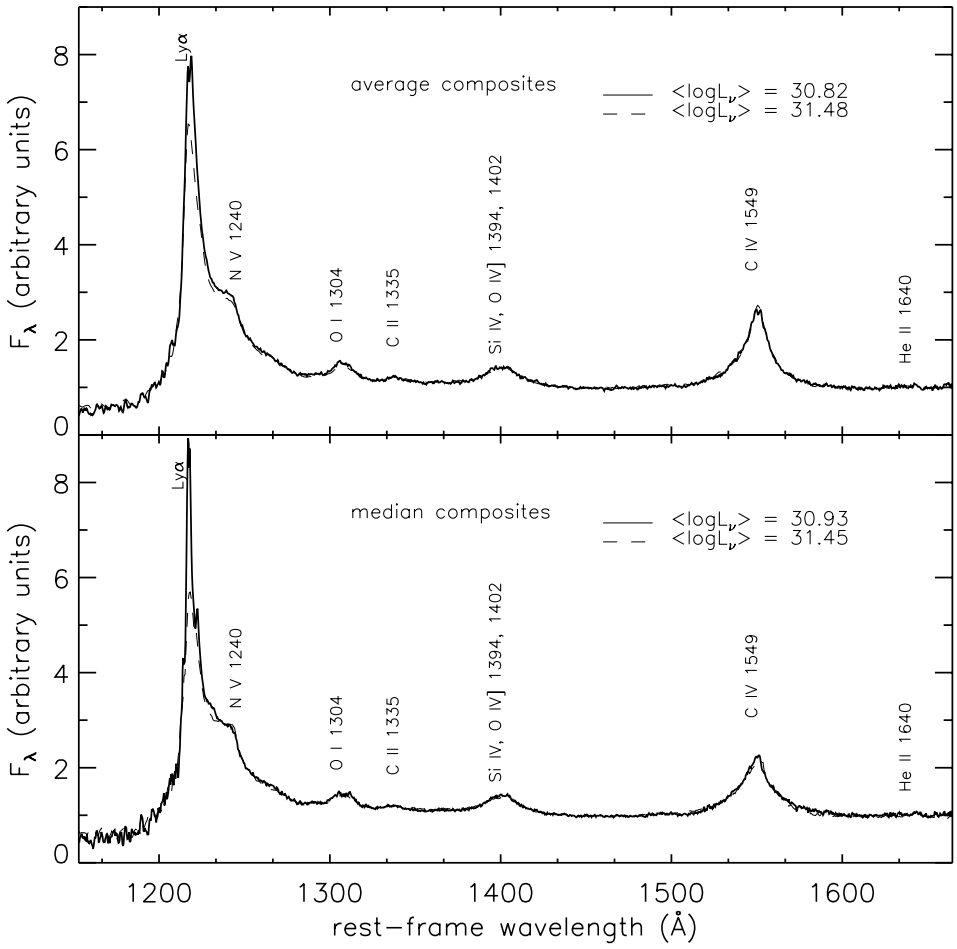

Fig. 7.— Comparison between median and average composites computed for two sets of quasars, grouped according to their luminosity at 1450Å (L_ν expressed in ergs s^{-1} Hz^{-1}). The same normalization as in Figure 2 is used. A weak drop in EW with luminosity can be noted for Lyα but not for C IV or other lines.

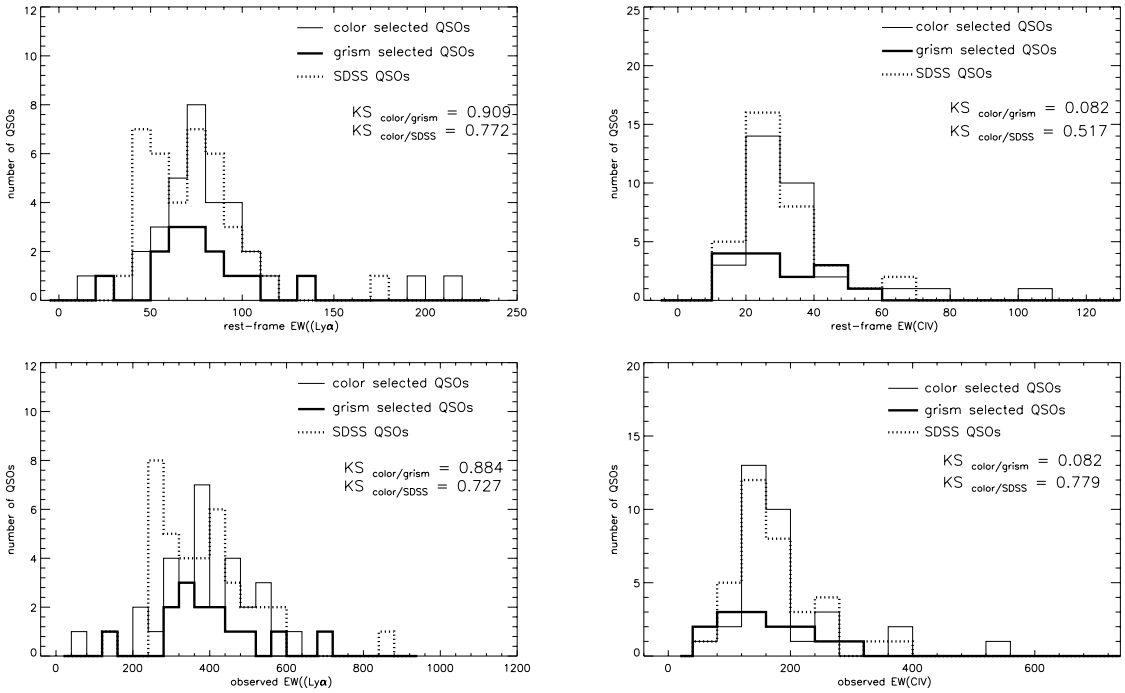

Fig. 8.— The distributions of the rest-frame (upper panels) and observed (lower panels) EWs for Lyα and C IV; three different samples are compared using a KS test criterion which indicates that the distributions are consistent with a common parent population.

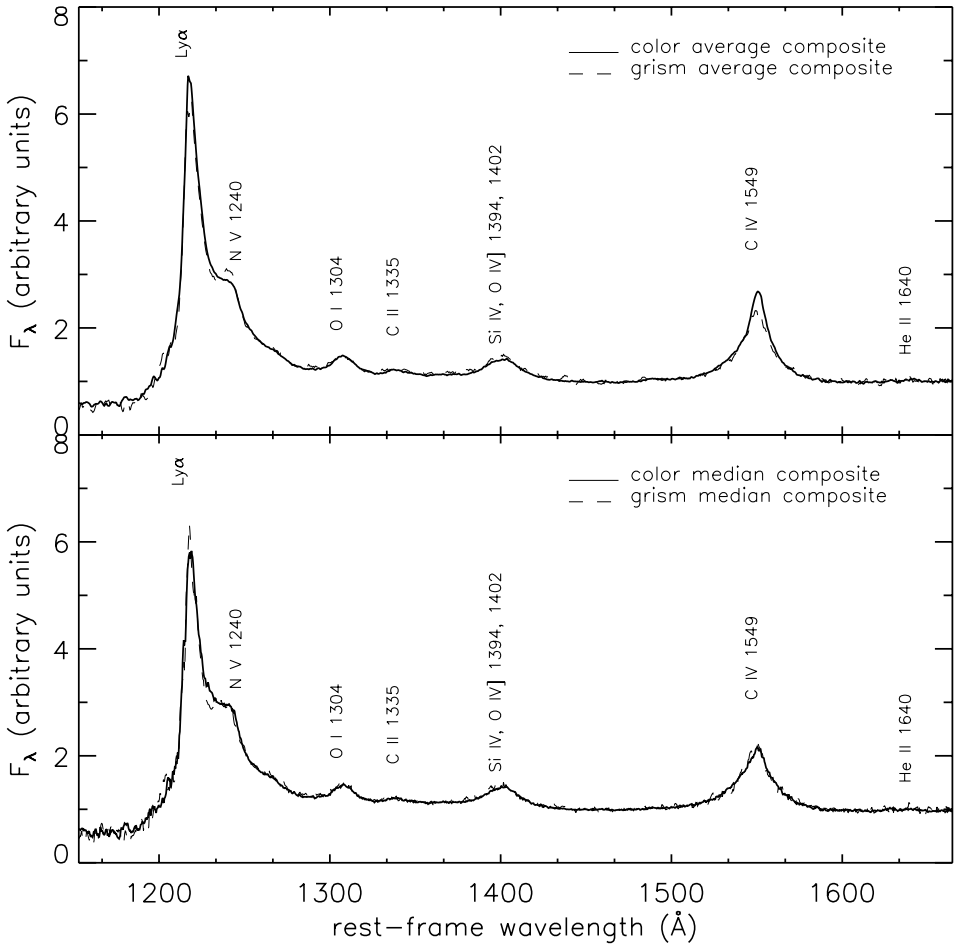

Fig. 9.— Comparison of composite spectra for color-selected and grism-selected QSOs. The composites include spectra published by SSG in addition to the data presented here. Average and median spectra are shown in the upper and lower panels, respectively.

TABLE 1
QSOs OBSERVED AT MMT AND KECK TELESCOPES.

Object	z[a]	r [b]	C IV		Lyα + N V	logL_ν(1450)	Ref
			EW$_1$[c](Å)	EW$_2$[d](Å)	EW[c](Å)		
PSS 0003+2730	4.23	19.3	33	32	95	31.30[f]	3
BR 0019-1522	4.52	19.0	43	34	97	31.53	6
PC 0027+0521	4.21	21.9	57	43	133	30.09	13
PC 0027+0525[e]	4.09	21.5	–	–	–		13
SDSS 003525+00	4.75	21.2	69	64	125	31.11	4
PSS 0059+0003	4.15	19.5	26	23	78	31.24[f]	7
BRI 0103+0032	4.43	18.6	44	36	87	31.52	15
PC 0131+0130	3.78	19.4	17	15	72	31.37	10
PSS 0137+2837[e]	4.30	19.0	–	–	–		3
BRI 0151-0025	4.19	18.9	–	–	72	31.44	15
PSS 0152+0735	4.05	19.6	27	27	60	31.06[f]	3
BRI 0241-0146	4.01	18.2	27	24	57	31.62	15
PSS 0248+1802	4.42	18.4	32	31	95	31.76[f]	8
PC 0307+0222	4.39	20.4	20	20	75	30.81	11
BR 0401-1711	4.22	18.7	68	61	195	31.49[f]	16
BR 0951-0450	4.34	18.9	28	28	66	31.35	9, 16
BRI 0952-0115	4.40	18.7	28	27	50	31.55	16
BRI 1013+0035	4.38	18.8	36	35	56	31.43	14
BR 1033-0327	4.49	18.5	26	24	72	31.53	6, 16
PSS 1048+4407[e]	4.45	19.3	–	–	–		8
BRI 1050-0000	4.28	18.7	73	73	119	31.26	14
PSS 1057+4555	4.10	17.7	24	21	74	31.79	8
BRI 1108-0747	3.91	18.1	28	25	93	31.44	16
BRI 1110+0106	3.91	18.3	20	19	42	31.40	16
BR 1144-0723[e]	4.16	18.6	–	–	–		16
PSS 1159+1337	4.08	18.5	–	–	15	31.91[f]	3
BR 1202-0725	4.69	18.7	17	17	22	31.87	6, 16
PC 1301+4747	3.99	21.3	46	46	27	30.32	12
PSS 1317+3531	4.36	19.1	30	29	85	31.39[f]	8
BRI 1328-0433	4.20	19.0	39	26	71	31.37	9, 16
BRI 1346-0322	4.00	18.8	–	–	104	31.21	16
PC 1415+3408	4.58	21.4	–	–	70	30.66	13
PSS 1435+3057	4.35	19.3	–	–	20		7
PSS 1438+2538[e]	4.24	19.5	–	–	–		8
PC 1450+3404	4.19	20.8	44	38	102	30.68	13
BRI 1500+0824	3.93	18.8	23	18	44	31.32	15
PSS 1618+4125	4.21	19.6	31	26	73	31.06[f]	3
Q 1745+6226	3.89	18.8	38	34	79	31.80[f]	1
RX 1759+6638	4.32	20.0	45	40	68	31.30	5
Q 2203+2900	4.41	20.8	31	26	53	30.87	2

TABLE 1—*Continued*

Object	z[a]	r [b]	C IV		Lyα + N V	logL_ν(1450)	Ref
			EW$_1$[c](Å)	EW$_2$[d](Å)	EW[c](Å)		
BR 2212-1626	3.99	18.1	51	50	87	31.53	16
BR 2237-0607	4.55	18.3	31	26	83	31.74[f]	6, 16
BR 2248-1242	4.15	18.5	106	98	211	31.24	6, 16
PC 2331+0216	4.09	20.0	17	15	85	30.93	11

[a]calculated from our spectra using the C IV emission-line

[b]photometry in r or analogous bandpass (R for the APM survey, r for PSS, r^* for SDSS, r_4 for SSG) as reported in the respective discovery papers

[c]rest-frame EWs calculated by direct integration of the line flux

[d]rest-frame EWs calculated by fitting the line to a single Gaussian

[e]exhibits broad absorption lines (BAL); z values are taken from the discovery papers

[f]values derived using the flux $f_\lambda(1450)$ measured from our spectra; estimated errors are approximately $\pm$ 0.2 dex.

REFERENCES.— (1) Becker et al. (1992); (2) Dickinson & McCarthy 1987; (3) S. Djorgovski, private comunication; (4) Fan et al. 1999; (5) Henry et al. 1994; (6) Isaak et al. 1994; (7) Kennefick et al. 1995a; (8) Kennefick et al. 1995b; (9) Kennefick et al. 1996; (10) Schmidt et al. 1987; (11) Schneider et al. 1989; (12) Schneider et al. 1991; (13) Schneider et al. 1997; (14) Smith et al. 1994a; (15) Smith et al. 1994b; (16) Storrie-Lombardi et al. 1996.